LA-UR- 11-04743

Approved for public release; distribution is unlimited.

Title:	SHOCK LOADING AND RELEASE OF A SMALL ANGLE TILT GRAIN BOUNDARY IN CU
Author(s):	Christian Brandl and Timothy C. Germann
Intended for:	Shock Compression of Condensed Matter, AIP Conf. Proc.

Los Alamos
NATIONAL LABORATORY
EST. 1943

Form 836 (7/06)

SHOCK LOADING AND RELEASE OF A SMALL ANGLE TILT GRAIN BOUNDARY IN CU

Christian Brandl* **and Timothy C. Germann***

**Los Alamos National Laboratory, Theoretical Devision, T-1, Los Alamos, NM 87545*

Abstract. Molecular dynamics simulations are performed to study the response of a dislocation tilt wall in Cu subjected to dynamic shock compression and release. We introduce a boundary condition for modeling the dynamics of a single interface subject to uniaxial loading parallel to the interface, avoiding artifacts from either periodic boundaries or free surfaces. The microstructure response for the small angle tilt boundary considered here is analyzed in terms of dislocation-dislocation interactions and the restoring forces which enable reversible dislocation motion upon release.

Keywords: Molecular dynamics,dynamic loading, Cu
PACS: 43.35.Ei, 78.60.Mq

INTRODUCTION

Previous molecular dynamics (MD) simulation studies of the shock response of crystalline solids have primarily concentrated on the macroscopic evolution (shock Hugoniot, stress state, and mode(s) of plastic deformation) and the determination of the Hugoniot elastic limit (HEL) in single crystals [1, 2, 3, 4]. However, realistic microstructures are usually polycrystalline, and more recently MD simulations have begun to examine the role of a single grain boundary (GB) structure on the dislocation nucleation process [5, 6, 7]. The collective role of GBs has also been investigated in nanocrystaline structures under dynamic loading conditions [8, 9]. Moreover, experimental work suggests that the local grain boundary structure may also determine the plastic deformation and failure responses in polycrystalline FCC materials in a nucleation-dominated regime. Pursuing this line of research, we present molecular dynamics simulations of a small angle grain boundary in copper to examine its response to shock loading and release.

METHOD

In our MD simulation setup (Fig. 1), the interface normal is parallel to the z axis and the shock direction is along the x axis. The two respective grains (upper and lower) are disoriented by $\approx 2.7°$ around the common [1 1 0] axis (y direction). The lattice directions are given in Table 1. Note that we have a quasi-2D simulation geometry due to the short periodic length in the y direction; further, an inspection of the lattice directions reveals that we have a symmetrical tilt grain boundary. The interatomic interaction is modeled by the embedded atom method (EAM) potential for Cu developed by Mishin et al [10]. In order to avoid the interaction of the interface with the corresponding interface between grains at a z periodic boundary, the typically used periodic boundary conditions are broken along the z direction. In the resulting free-surface region (15 Å thick; grey region in Fig. 1) the atoms are constrained to move according the forces within xy-plane, but are not allowed to move in the z direction. Periodic boundary conditions are only imposed along the y-direction (tilt axis). Therefore lateral relaxation during the shock loading is suppressed, whilst the shock

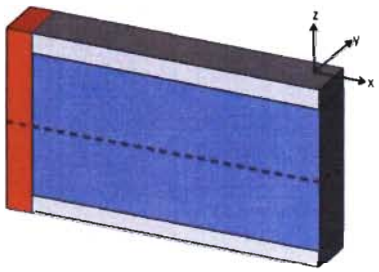

FIGURE 1. Schematic of the bicrystal simulation geometry. The interface (parallel to the xy-plane) is indicated by a black dashed line. The shock is imposed by a constant velocity piston region - indicated by the red volume. Periodic boundary conditions are imposed along the y-direction. The atoms in the grey sub-volume are confined to move only in the xy-plane.

dynamics are only marginally affected. This simulation geometry allows us to study the response of a well-controlled grain boundary (or interface) structure without introducing artifacts from either periodic (uncontrolled, and usually high energy) interface structures, or free surfaces. The compressive shock wave is generated by a constant velocity ($u_p = v_x = 200$ m/s) piston region - illustrated as the red region in Fig. 1. The microstructural evolution is analyzed using

- the atomic virial stress due to the interatomic forces [11], assuming the zero strain atomic volume of FCC Cu; and
- common neighbor analysis [12].

The color schema are described in the corresponding figure captions. The atomistic configurations are visualized using OVITO [13]. After geometrical construction of the bicrystal, the conjugate gradient method is used to relax the atomic positions towards a zero stress state. The atomic positions (and simulation box) are subsequently rescaled based on the known thermal expansion, and equilibrated at 100 K resulted in a stress free configuration in the bulk regions of the two grains. The atomic trajectories are integrated with an NVE ensemble subject to the aforementioned boundary conditions. The MD simulations use the LAMMPS simulation package [14].

TABLE 1. Orientation of the lower and upper grain (see Fig. 1)

direction	lower grain	upper grain	length
x	[1 -1 60]	[-1 1 60]	≈ 217 nm
y	[1 1 0]	[1 1 0]	≈ 0.5 nm
z	[-30 30 1]	[-30 30 -1]	≈ 31 nm

RESULTS

Interface structure

Fig. 2 shows the details of dislocation wall after equilibration using the dislocation analysis of Stukowski et al [15] . In Fig. 2a the dislocation cores are shown as lines which are colored according to the Burgers vector magnitude (in Å). The connecting stacking faults appear as red planes. Fig. 2b shows a representative cross section of the initial atomistic configuration. Both structure representations reveal that the dislocation wall consists of two different sets of partial dislocations, whose habit planes have a common intersection with the [1 1 0] tilt axis. Note as well that the habit plane is close to an high Schmidt factor orientation. Moreover, different dislocation core configurations appear which may be categorized into: (1) fully separated dissociated full dislocations (beige colored lines in Fig. 2a) , (2) formation of a super jog (red colored lines in Fig. 2a), and (3) formation of a stair rod dislocation (blue colored lines in Fig. 2a) [16].

Shock response

Fig. 3 shows an x-t diagram of the shear stress evolution (color scale in GPa) during the shock loading and subsequent release. During the shock loading stage (until 47 ps), the shock front rises the stress state (to ≈ 1 GPa shear stress) followed by the stress relaxation to roughly ≈ 0.6 GPa. Note that the dislocation motion is limited by the imposed boundary conditions, and it is not known whether an even larger grain size would permit a greater degree of shear stress relaxation.

Fig. 4 further illustrates the temporal evolution by showing only non-FCC atoms (in color) superimposed on the shear stress field (grey atoms). We note

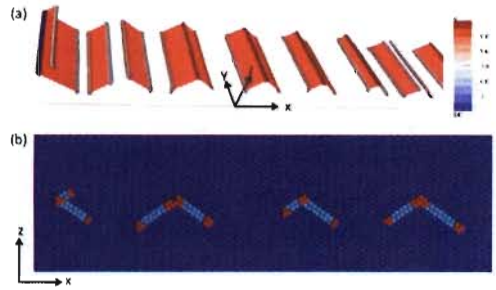

FIGURE 2. a) Extracted dislocation structure from the initial micro structure. The solid lines represent the dislocation cores, colored according to their Burgers vector magnitude (see colorbar). The stacking faults are the red and transparent planes. b) Details of the atomistic initial microstructure. The atoms are colored according to their local crystalline structure; FCC, HCP and others in blue, cyan and red, respectively.

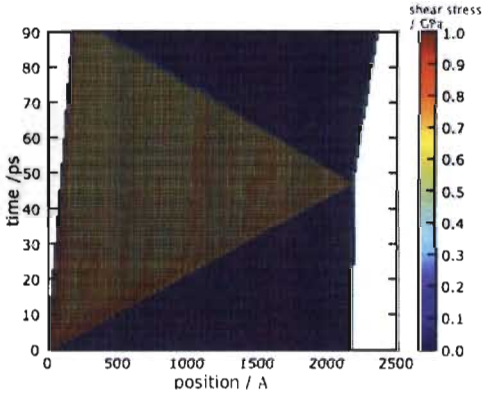

FIGURE 3. Shear stress evolution during shock loading and release, as an x-t diagram. The shear stress τ is computed from the diagonal stress tensor components ($2\tau = \sigma_{xx} - 1/2(\sigma_{yy} + \sigma_{zz})$) for a cross section volume in the shock front plane (yz-plane). The colors indicate the local shear stress in GPa.

that the onset of dislocation propagation is slightly behind the shock front. Since the shear stress is not instantaneously relaxed by dislocation motion, the shock wave elastically overloads the sample (red regions in Fig. 3). Furthermore, the activated dislocation motion is not symmetric in respect to the initial GB plane. This might be attributed to the shadowing effect, which results from two factors. First, a previously propagated dislocation relaxes the shear stress and therefore lowers the applied shear stress at an adjacent GB dislocation. And second, dislocations with the same Burgers vector repel each other. However, in general the mobile dislocation density, which is imposed by the interface structure, effectively lowers the shear stress state by propagation of a constituent partial dislocation. Because the trailing partial dislocations remain approximately at their initial locations, this gives rise to an restoring force in terms of a widening of the stacking fault region. During the release phase (times longer than ≈ 47 ps), the stacking faults pull back the leading partial dislocation to the initial interface plane (see Fig. 4). Via this reversible dislocation motion, the shocked sample unloads to approximately a zero shear stress state. Finally, we note that the novel boundary conditions which we have introduced do not appear to alter the planar nature of the shock front.

DISCUSSION / SUMMARY

In summary, we have presented the inelastic deformation behavior of a symmetric-tilt small angle GB subjected to shock compression and release using MD simulations. During the compressive loading phase, the motion of leading partial dislocations enables the shear stress relaxation of the surrounding grains. Upon rarefaction, the extended stacking faults enable the reversible dislocation motion. More generally, the preexisting mobile dislocation density within a general grain boundary can effectively accommodate the compressive loading conditions towards an isotropic stress state. The reversible dislocation motion presented here surely does not cover the effect of the dislocation density coming from the bulk regions and their interaction with the dislocation wall. Moreover, the reversibility may also be caused by the planar nature of dislocation tilt wall, and hence does not account for pinning effects imposed by cross-slip, dislocation intersections, and tangling [3]. Future simulation studies will address the preexisting dislocation content on the shock response of grain boundaries, the effect of impinging dislocations on GB response, and the effect of reversible dislocation motion in the presence of intersecting dislocations.

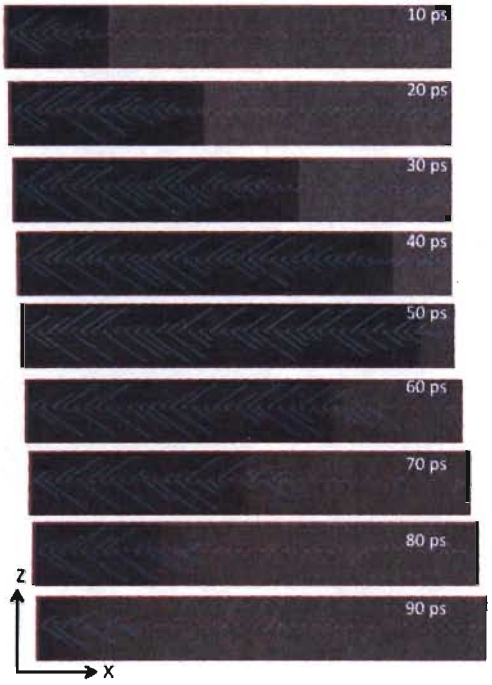

FIGURE 4. Defect evolution during shock loading and subsequent release. Non-FCC atoms (colored atoms; cyan=HCP, red= other atoms) are shown superimposed on the cross-section of the atomic stress (σ_{xx}) in a grey scale ranging from -10 GPa (black) to 10 GPa (white).

ACKNOWLEDGMENTS

This work was supported by the Center for Materials at Irradiation and Mechanical Extremes, an Energy Frontier Research Center funded by the U.S. Department of Energy, Office of Science, Office of Basic Energy Sciences under Award Number 2008LANL1026.

REFERENCES

1. Meyers, M. A., Jarmakani, H., Bringa, E. M., and Remington, B. A., "Chapter 89 Dislocations in Shock Compression and Release," in *Dislocations in Solids*, edited by J. Hirth and L. Kubin, Elsevier, 2009, vol. 15, pp. 91 – 197.
2. Kadau, K., Germann, T. C., Lomdahl, P. S., Albers, R. C., Wark, J. S., Higginbotham, A., and Holian, B. L., *Phys. Rev. Lett.*, **98**, 135701 (2007).
3. Germann, T. C., Tanguy, D., Holian, B. L., Lomdahl, P. S., Mareschal, M., and Ravelo, R., *Metal. and Mater. Trans. A*, **35**, 2609–2615 (2004).
4. Bringa, E. M., Rosolankova, K., Rudd, R. E., Remington, B. A., Wark, J. S., Duchaineau, M., Kalantar, D. H., Hawreliak, J., and Belak, J., *Nat. Mater.*, **5**, 805–809 (2006).
5. Pozzi, C., Germann, T. C., and Hoagland, R. G., "Molecular dynamics simulation of dislocation emission from shocked Aluminium grain boundaries," in *Shock Compression of Condensed Matter*, edited by Elert, M L and Buttler, W T and Furnish, M D and Anderson, W W and Proud, W G, 2009, vol. 1195 of *AIP Conf. Proc.*, pp. 765–768.
6. Dremov, V. V., Sapozhnikov, P. A., and Bringa, E. M., "Molecular dynamics simulation of interaction between shock wave and high-symmetry intergranular boundary," in *Shock Compression of Condensed Matter*, edited by Furnish, M D and Elert, M and Russell, T P and White, C T, 2006, vol. 845 of *AIP Conf. Proc.*, pp. 387–390.
7. Luo, S.-N., Germann, T. C., Tonks, D. L., and An, Q., *J. Appl. Phys.*, **108**, 093526 (2010).
8. Bringa, E. M., Caro, A., Wang, Y., Victoria, M., McNaney, J. M., Remington, B. A., Smith, R. F., Torralva, B. R., and Van Swygenhoven, H., *Science*, **309**, 1838–1841 (2005).
9. Luo, S.-N., Germann, T. C., Desai, T. G., Tonks, D. L., and An, Q., *J. Appl. Phys.*, **107**, 123507 (2010).
10. Mishin, Y., Mehl, M. J., Papaconstantopoulos, D. A., Voter, A. F., and Kress, J. D., *Phys. Rev. B*, **63**, 224106 (2001).
11. Thompson, A. P., Plimpton, S. J., and Mattson, W., *J. Chem. Phys.*, **131**, 154107 (2009).
12. Honeycutt, J. D., and Andersen, H. C., *J. Phys. Chem.*, **91**, 4950–4963 (1987).
13. Stukowski, A., *Modelling Simul. Mater. Sci. Eng.*, **18**, 015012 (2010).
14. Plimpton, S. J., *J. Comput. Phys.*, **117**, 1–19 (1995).
15. Stukowski, A., and Albe, K., *Modelling Simul. Mater. Sci. Eng.*, **18**, 085001 (2010).
16. Hirth, J. P., and Lothe, J., *Theory of Dislocations*, Krieger Publishing Company, 1992, 2nd edn.